

## Structure and spectroscopy of two new bases for building block: Terpyridine derivatives



Dominique Toledo <sup>a</sup>, Ricardo Baggio <sup>b</sup>, Eleonora Freire <sup>b,c</sup>, Andrés Vega <sup>d</sup>, Nancy Pizarro <sup>e</sup>, Yanko Moreno <sup>d,\*</sup>

<sup>a</sup> Departamento de Química, Universidad de Concepción, Chile

<sup>b</sup> Gerencia de Investigación y Aplicaciones, Centro Atómico Constituyentes, Comisión Nacional de Energía Atómica, Buenos Aires, Argentina

<sup>c</sup> Universidad Nacional San Martín, Buenos Aires, Argentina

<sup>d</sup> Universidad Andrés Bello, Facultad de Ciencias Exactas, Departamento de Química, Quillota 980, Viña del Mar, Chile

<sup>e</sup> Universidad Andrés Bello, Facultad de Ciencias Exactas, Departamento de Química, Republica 275, Santiago, Chile

### ARTICLE INFO

#### Article history:

Received 18 June 2015

Received in revised form

6 August 2015

Accepted 13 August 2015

Available online 19 August 2015

#### Keywords:

Molecular structure

Fluorescence

Terpyridine

TDDFT analysis

### ABSTRACT

Two new terpyridine compounds are reported: 4'-(3-methyl-2-thienyl)-4,2':6',4''-terpyridine, C<sub>20</sub>H<sub>15</sub>N<sub>3</sub>S, (**I**) and 4'-(4-quinolinyl)-4,2':6',4''-terpyridine, C<sub>25</sub>H<sub>17</sub>C<sub>13</sub>N<sub>4</sub>, (**II**). Both structures crystallize in centrosymmetric space groups and present weak H-bonds, which gives greater stability to their structures. Light absorption by both molecules is firmly established on the experimental and the TDDFT analysis as coming from  $\pi \rightarrow \pi^*$  transitions. The fluorescence of both compounds has a small Stokes shift, which is also consistent with the emission from highly rigid molecules. Furthermore, the thermal stability observed for both compounds, until about 280 °C, making these molecules interesting candidates for use as complex ligands, which are obtained by means of solvothermal synthesis (technique with temperatures of about 150 °C).

© 2015 Published by Elsevier B.V.

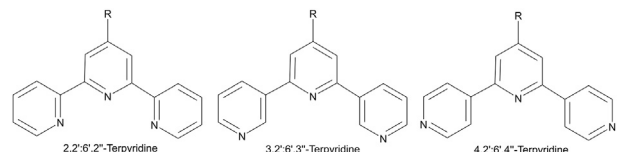
### 1. Introduction

One of the first steps in metallosupramolecular chemistry is to find versatile building blocks [1–6]. On the other hand, much effort has been focused on the purposeful design and controllable synthesis of coordination systems employing multidentate ligands [7–10]. Systems such as pyridine, 2,2'-bipyridine, 1,10-phenanthroline or similar have a desired ability to coordinate hard and medium metal ions; then, the formed structures are stabilized thanks to the pi conjugated system and also due to its aromatic ring stacking. However, these systems are discrete in nature. In order to obtain a chain or planar type system, it is required a ligand wherein the donor atoms arrangement ensures the spread of the molecular structure: this requirement is met by some terpyridines.

Along the years, n,2':6',n'' Terpyridines (Tpy) as well as all their 4'-substituted derivatives have been the subject of intensive structural study, in any of their current forms, viz., n = 2, 3 and 4 (**Scheme 1**).

The different spatial disposition of the nitrogen donors in these forms confers them a striking diversity of coordinative capabilities, as a search in the CSD (v5.13 plus Feb. 2014 updates [11]) easily discloses. **Table 1** presents a summary of the results obtained for the three types of Tpy-based compounds, pointing out the number of reported moieties, either complexes or unbound, and among the former, the polymeric ones are prominent.

The most numerous, by far, is the 2,2':6',2'' group that coordinates almost exclusively as  $\mu_1\kappa^3$  chelating ligands due to the convergent disposition of the N donors. The few polymeric reported cases are the result of the bridging capabilities of the eventual R substituent. On the other hand, the 3,2':6',3'' group is the less frequently reported; the stereo-disposition of the pyridyl



**Scheme 1.** 2,2':6',2'', 3,2':6',3'' and 4,2':6',4''-terpyridine molecules.

\* Corresponding author.

E-mail address: [yanko.moreno@unab.cl](mailto:yanko.moreno@unab.cl) (Y. Moreno).

**Table 1**

Number of terpyridine based structures in the CSD [11].

Tpy type	Uncomplexed	Complexed (Any metal)	Complexed (Polymeric)	Polymeric percentage
2,2':6',2''-	114	678	136	20%
3,2':6',3''-	2	11	8	73%
4,2':6',4''-	10	61	54	89%

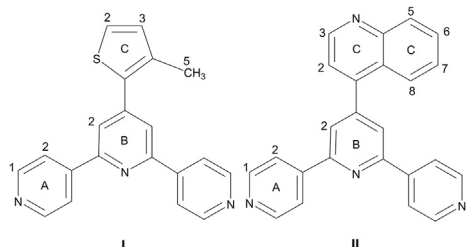
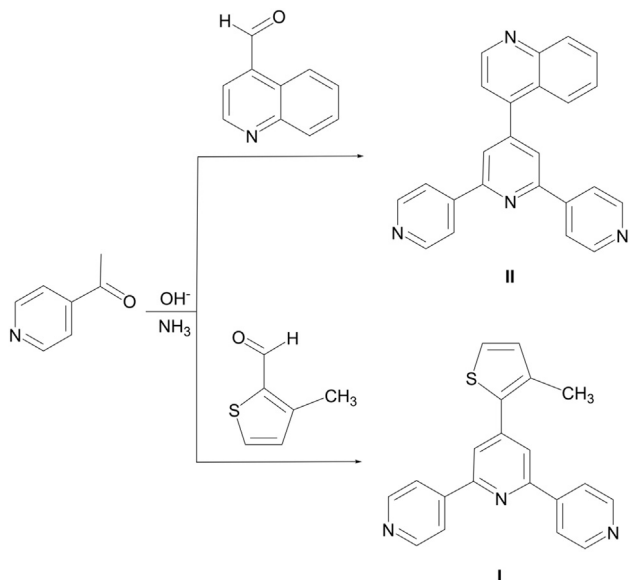
N's, somehow intermediate between the other two, allows both monomeric as well as polymeric coordination arrangements. Finally, the 4,2':6',4'' case ranks second in the number of entries, though far from the 2,2'. All these ligands appear as very versatile in their coordination modes: their divergent nature allows them to connect to metal centers acting either as bidentate-bridging (using the 4,4''-pyridyl groups to give an infinite chain structure [3,4,6] or a 3D network structure [8]) or as tridentate (using the three external 4-pyridyl groups to engage in a 3D structural motif [9] or molecular capsules [7]). This versatility turns this type of ligands particularly attractive for the generation of complex networks, in particular open 3D coordination structures (metal-organic framework, MOF's). Their particular structural nature and versatile coordination possibilities of these ligands could lead to interesting physical properties such as luminescence [12,13] or the cooperative type, as the magnetic ones [14–16]. The aim of our research line is to obtain ligands that result in complexes with cooperative magnetic properties.

As an initial step in order to explore new 4,4'' divergent terpyridine-based ligands and further analyze their coordination capabilities and supramolecular properties, we present herein two new free ligands (**Scheme 2**) obtained when changing the R substituent, viz.: 4'-(3-methyl-2-thienyl)-4,2':6',4''-terpyridine (**I**) and 4'-(4-quinolinyl)-4,2':6',4''-terpyridine (**II**).

Both structures crystallize in centrosymmetric space groups P2<sub>1</sub>/n for **I** and P1 for **II**; with one single molecule per asymmetric unit. We have studied the fluorescence behavior for both systems, in order to eventually compare, with the respective transition metal complexes for these compounds. With this in mind, we have studied the absorption and emission spectra for both systems; indicating that this electronic transitions are  $\pi \rightarrow \pi^*$  type. Then, as mentioned before, the expected continuity is to obtain coordination compounds, considering that these ligands are thermally stable up to about 280 °C the solvothermal synthesis techniques could also be implemented.

## 2. Experimental

**i.- Syntheses.** The terpyridine systems were prepared according to the Aldol condensation and Michael addition [17] methods (**Scheme 3**) with minimal modifications; the chemical reagents were used without further purification.

**Scheme 2.** Molecular structure diagram for **I** and **II**, with ring labeling and numbering.**Scheme 3.** Synthetic pathway for **I** and **II**.

**4'-(3-methyl-2-thienyl)-4,2':6',4''-terpyridine (I).** 4-acetylpyridine (1.211 g, 10 mmol) was added to 25 mL of 3-methylthiophenecarboxaldehyde ethanolic solution (0.6309 g, 5 mmol). The solution was stirred for 10 min, then KOH (0.5611 g, 10 mmol) and concentrated NH<sub>3</sub> were added (14.5 mL). The mixture was stirred overnight (ca.18 h). A yellow precipitate was obtained and then filtered and washed with water (4 × 10 mL). Recrystallization of the ligand was done in CH<sub>3</sub>Cl (15 mL). Pale yellow needles were obtained: C<sub>20</sub>H<sub>15</sub>N<sub>3</sub>S (770 mg, 2.337 mmol, 46.74%). *Anal.* Calc: C, 72.92; H, 4.59; N, 12.76; S, 9.73. Found: C, 73.0; H, 4.7; N, 13.0; S, 9.5.

**<sup>1</sup>H NMR** (400 MHz, CDCl<sub>3</sub>) δ 8.79 (d, J = 6.0 Hz, 4H, H<sup>A1</sup>), 8.04 (d, J = 6.0 Hz, 4H, H<sup>A2</sup>), 7.91 (s, 2H, H<sup>B2</sup>), 7.40 (d, J = 5.0 Hz, 2H, H<sup>C2</sup>), 7.04 (d, J = 5.0 Hz, 2H, H<sup>C3</sup>), 2.50 (s, 3H, H<sup>C5</sup>). **<sup>13</sup>C NMR** (101 MHz, CDCl<sub>3</sub>) δ 155.13 (C<sup>B1</sup>), 150.60 (C<sup>A1</sup>), 145.89 (C<sup>A3</sup>), 145.03 (C<sup>B3</sup>), 136.14 (C<sup>C1</sup>), 134.17 (C<sup>C4</sup>), 132.01 (C<sup>C3</sup>), 125.94 (C<sup>C2</sup>), 121.16 (C<sup>A2</sup>), 120.10 (C<sup>B2</sup>), 15.50 (C<sup>C5</sup>).

**FT-IR** (KBr, cm<sup>-1</sup>) 3085, 3026 (merged ν<sub>CH</sub> pyridine and thiophene rings), 2976 (ν<sub>CH</sub> methyl), 1591, 1539 and 1400 (ν<sub>CC</sub> pyridine and thiophene rings), 1065(w), 996(w), 826(m), 739(m), 629(m), 490(w).

**4'-(4-quinolinyl)-4,2':6',4''-terpyridine (II).** 4-acetylpiridina (0.9691 g, 8 mmol) was added to 20 mL of 4-quinolinylcarboxaldehyde ethanolic solution (0.6287 g, 4 mmol). The solution was stirred by 10 min, then KOH (0.449 g, 8 mmol) and concentrated NH<sub>3</sub> were added (11.6 mL). The mixture was stirred ca 4 h. A white precipitate was obtained and then filtered and washed with water (3 × 10 mL) and ethanol (2 × 10 mL).

Recrystallization of the ligand was done in CH<sub>3</sub>Cl (18 mL). White crystals plates were obtained: C<sub>24</sub>H<sub>16</sub>N<sub>4</sub> (750 mg, 2081 mmol, 39.08%). *Anal.* Calc: C, 79.98; H, 4.47; N, 15.55. Found: C, 78.0; H, 4.3; N, 15.0.

**<sup>1</sup>H NMR** (400 MHz, CDCl<sub>3</sub>) δ 9.06 (d, J = 4.2 Hz, 1H, H<sup>C3</sup>), 8.80 (d, J = 6.0 Hz, 4H, H<sup>A1</sup>), 8.26 (d, J = 8.4 Hz, 1H, H<sup>C5</sup>), 8.09 (d, J = 6.0 Hz, 4H, H<sup>A2</sup>), 8.00 (s, 2H, H<sup>B2</sup>), 7.83 (dd overlapping, J = 14.8, 8.0 Hz, 2H, H<sup>C6/C8</sup>), 7.60 (t, J = 7.6 Hz, 1H, H<sup>C7</sup>), 7.45 (d, J = 4.2 Hz, 1H, H<sup>C2</sup>).

**<sup>13</sup>C NMR** (101 MHz, CDCl<sub>3</sub>) δ 155.26 (C<sup>B1</sup>), 150.72 (C<sup>A1</sup>), 150.01 (C<sup>C3</sup>), 148.73 (C<sup>C4</sup>), 148.61 (C<sup>C9</sup>), 145.44 (C<sup>A3</sup>), 145.06 (C<sup>B3</sup>), 130.41 (C<sup>C5</sup>), 130.06 (C<sup>C6/C8</sup>), 127.70 (C<sup>C7</sup>), 125.70 (C<sup>C1</sup>), 124.73 (C<sup>C6/C8</sup>), 121.25 (C<sup>C2</sup>), 121.16 (C<sup>A2</sup>), 120.93 (C<sup>B2</sup>).

**FT-IR** (KBr,  $\text{cm}^{-1}$ ) 3029.53 (merged  $\nu_{\text{CH}}$  pyridine and quinoline rings), 1590, 1543, 1432 and 1391 ( $\nu_{\text{CC}}$  pyridine and quinoline rings), 1065(w), 986(w), 836(m), 756(s), 627(m).

**NMR spectroscopy.**  $^1\text{H}$  and  $^{13}\text{C}$  NMR spectra in  $\text{CDCl}_3$  solution were recorded on a Bruker-400 NMR spectrometer (chemical shifts referenced to residual solvent peaks, TMS =  $\delta$  0).

**Infrared spectra.** Infrared spectra were obtained from KBr pellets on a Bruker EQUINOX 55 Fourier transform infrared spectrometer in the 400–4000  $\text{cm}^{-1}$  region.

### 3. Spectroscopic and photophysical measurements

#### 3.1. Steady state absorption

UV–Vis absorption spectra of compounds I and II in air-saturated  $\text{CH}_2\text{Cl}_2$  solutions were recorded on an Agilent 8453 Diode-Array spectrophotometer in the range of 250–800 nm. Molar absorptivity was determined according to Lambert–Beer Law by measuring absorbance at 272 nm and 307 nm for different concentrations of solutions ranging from 1  $\mu\text{M}$  to 20  $\mu\text{M}$ .

#### 3.2. Steady state emission

Emission spectra of compounds I and II in air-saturated  $\text{CH}_2\text{Cl}_2$  solutions were measured in a Horiba Jobin–Yvon FluoroMax-4 spectrofluorometer at room temperature. Quantum yields of luminescence were measured at room temperature using quinine sulfate in 0.1 M  $\text{H}_2\text{SO}_4$  (quantum yield ( $\Phi_{\text{em}}$ ) = 0.546 for excitation at 350 nm) [18] as actinometer. Other solvents like MeCN and EtOH, were also employed in order to observe the solvent polarity effect.

#### 3.3. Time resolved emission

Luminescence decay curves were recorded using the time-correlated single photon counting technique in a PicoQuant Fluotime 300 fluorescence lifetime spectrometer. A sub-nanosecond Pulsed LED PLS-330 was employed as the pulsed light source (FWHM ~ 500 ps; average power 10 MHz).

#### 3.4. Thermogravimetric analysis

Thermogravimetric analysis (TGA) were carried out with a Universal V2.6 DTA system at a rate of 10 °C/min in a nitrogen atmosphere.

#### 3.5. Single crystal structure determination

For both crystals, crystal data were collected on Oxford Gemini [19] CCD S Ultra diffractometer at room temperature using Mo K $\alpha$  radiation ( $\lambda = 0.71073 \text{ \AA}$ ). The structures were solved by direct methods and refined by full-matrix least squares on  $F^2$  using the SHELXS-97 [20] software. All non-hydrogen atoms were refined

anisotropically. The structural analysis was performed with the help of the multipurpose PLATON [21] program and the molecular representations shown in the figures were generated using XP in the SHELXTL [22] package. All H atoms were found in a difference map, being further idealized and finally allowed to ride with  $d_{\text{C}-\text{H}} = 0.93 \text{ \AA}$  and  $U_{\text{iso}}(\text{H}) = 1.2 U_{\text{eq}}(\text{C})$ . Data collection and refinement parameters are summarized in Table S1, in Supporting information.

#### 3.6. Computational calculations

All geometry optimizations were performed at the B3LYP/6-31 + G(d,p) level of theory using the Gaussian09 Rev C.01 package of programs (G09) [23], and started from geometry determined by means of x-ray diffraction.

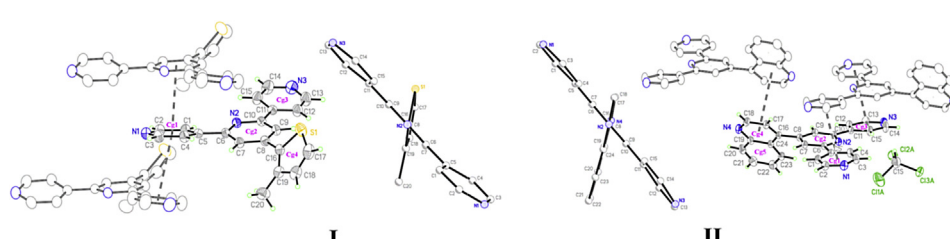
### 4. Results and discussion

#### 4.1. Structural description

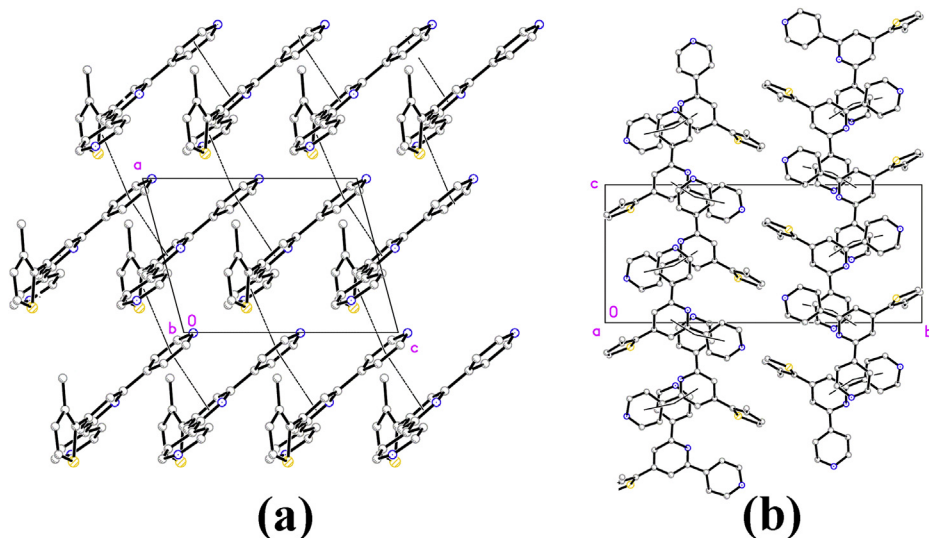
Fig. 1 presents ellipsoid plots for I and II, showing the labeling scheme used. Both structures crystallize in centrosymmetric space groups  $P2_1/n$  for I and  $P\bar{1}$  for II; with one single molecule per asymmetric unit. II includes a slightly disordered trichloromethyl solvate molecule as a part of its packing structure. The terpyridine core is not planar for each molecule, having the pyridine rings arms 1 and 3 (see Scheme 1 for labeling) being significantly rotated with respect to the central one (2).

Fig. 1 (center) gives a clear view of this fact, by showing a projection of both structures down the N2–C8 line in the Py(2) ring; the larger departure from planarity for I is apparent, as disclosed by the interplanar angles between pyridine rings, in I, II sequence: 18.12(12)°, 5.35(15)° for (2:1) and 10.06(13)°, 7.24(16)° for (2:3). The main distortion, anyway, resides in the (2:4) dihedral angle subtended by the planar substituents R, rotated in turn by 51.85(12), 53.40(16)°, again in I and II sequence. Internal bond distances and angles do not depart from expected values, and the most interesting aspect of both structures resides in their supramolecular structure, driven by extremely weak  $\pi \cdots \pi$  and C–H $\cdots$  $\pi$  interactions. While the most significant non covalent interactions are presented in Table S3 ( $\pi \cdots \pi$  contacts) and Table S4 (H-bonds). In compound I the only relevant ones are two  $\pi \cdots \pi$  bonds having py(1) in common (Table S3 and Fig. 1).

These contacts link molecules into broad 2D structures parallel to (010) (Fig. 2a) with very weak interactions between them (Fig. 2b). In the case of compound II, there are two types of relevant interactions, fulfilling a quite different role each. Table S3 presents two  $\pi \cdots \pi$  contacts linking molecules into strips parallel to <110> (Fig. 3a). These 1D units, in turn, are interconnected in two almost perpendicular directions by the C–H $\cdots$  $\pi$  bonds described in Table S4 and shown in Fig. 3b. The one involving H22 links strips (coming out of the paper in Fig. 3b) roughly along <001>



**Fig. 1.** Ellipsoid plots for I (left) and II (right). Midway, similar projections done the N2–C8 line, showing the respective distortions from planarity.



**Fig. 2.** Packing views of I. (a) Projected down <010>, showing the full 2D structure build up by  $\pi \dots \pi$  bonds. (b) Projected down <100>, with planes viewed sideways, showing the weak interaction between them.

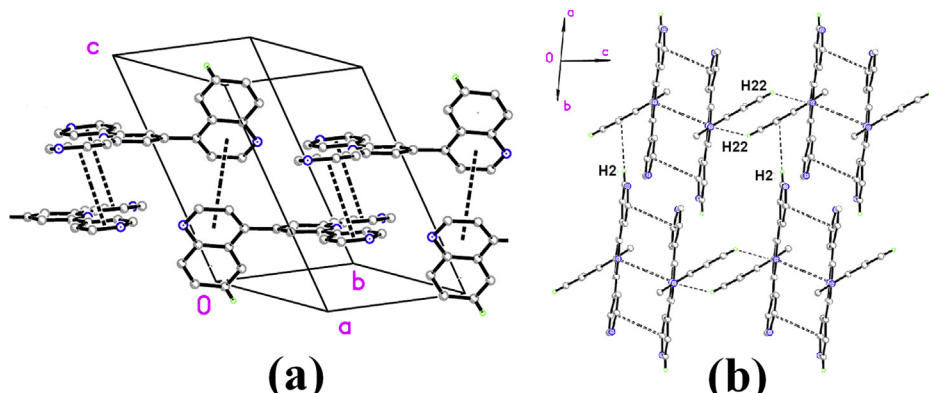


**Fig. 3.** Packing views of II. (a) Projected down <-110>, showing the way in which strips are built up via  $\pi \dots \pi$  bonds. (b) Projected down the strips direction, showing the two types of lateral C-H... $\pi$  bonds joining strips into a 3D structure.

(horizontally in the figure). The one involving H2, instead (almost vertical in the figure), link the 2D substructures thus formed into the final 3D supramolecular arrangement.

#### 4.2. Magnetic resonance studies

$^1\text{H}$  NMR (Fig. S2), and  $^{13}\text{C}$ -NMR (Fig. S3) spectra were assigned

using routine 2D methods and these are consistent with the proposed structures. In the  $^1\text{H}$  NMR spectra the splitting pattern of the fragment corresponding 4,2'-6',4''-terpyridine (AB-Pattern doublets for protons  $\text{H}^{\text{A}1}$ ,  $\text{H}^{\text{A}2}$  and  $\text{H}^{\text{B}2}$ ) is observed in both cases with similar chemical shift, approximately at  $\delta = 8.80$ , 8.00 and 7.90 ppm. As expected, the change of substituent gives rise to the corresponding signals for thiophene and quinoline rings. The  $^1\text{H}$

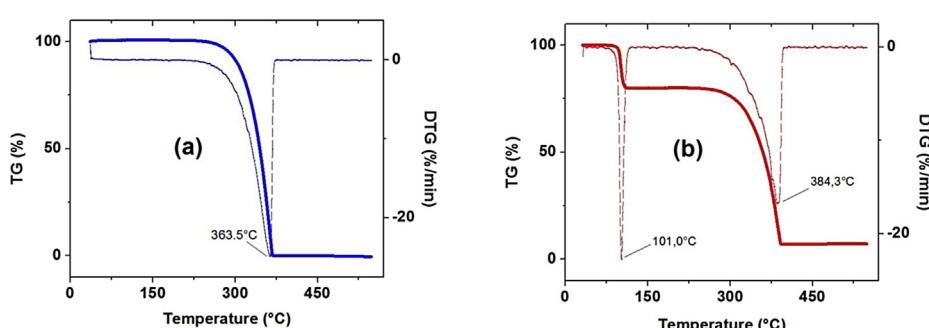


**Fig. 4.** TGA and DSC for a) I and b) II.

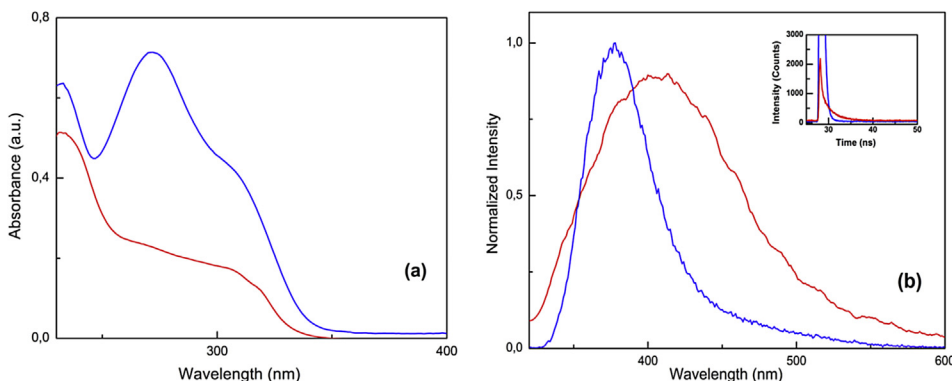


**Fig. 5.** a.- Absorption spectra and b.- Emission spectra of ligands **I** (blue line) and **II** (red line) in air-saturated  $\text{CH}_2\text{Cl}_2$  solutions. **Inset:** Emission decays upon excitation at 330 nm (For interpretation of the references to colour in this figure legend, the reader is referred to the web version of this article.).

NMR spectrum of **I** is characterized for a high field singlet at 2.50 ppm, due to the three protons ( $\text{H}^{\text{C}5}$ ) of the methyl group. For **II**, an overlapping of signals occurred for the  $\text{H}^{\text{C}6}$  and  $\text{H}^{\text{C}8}$  protons (doublet of doublets at 7.83 ppm), but all quinoline protons can be readily distinguished using COSY and HSQC experiments. Similarly, the  $^{13}\text{C}$  NMR spectrum shows the corresponding signals of the fragment 4,2',6',4''-terpyridine in the aromatic region: three due to quaternary carbons at approximately 155.20 ( $\text{C}^{\text{B}1}$ ), 146.00 ( $\text{C}^{\text{A}3}$ ) and 145.00 ( $\text{C}^{\text{B}3}$ ) ppm and three due to CH carbons at approximately 150.60 ( $\text{C}^{\text{A}1}$ ), 121.16 ( $\text{C}^{\text{A}2}$ ) and 120.10 ( $\text{C}^{\text{B}2}$ ) ppm. In the  $^{13}\text{C}$  NMR spectrum of **I** can be distinguished one solitary methyl group at 15.50 ppm ( $\text{C}^{\text{C}5}$ ). And for **II** is observed two signals due to quaternary carbons at 148.73 ( $\text{C}^{\text{C}4}$ ), 148.61 ( $\text{C}^{\text{C}9}$ ) ppm and seven due to CH carbons at 150.01 ( $\text{C}^{\text{C}3}$ ), 130.41 ( $\text{C}^{\text{C}5}$ ), 130.06 ( $\text{C}^{\text{C}6/\text{C}8}$ ), 127.70 ( $\text{C}^{\text{C}7}$ ), 125.70 ( $\text{C}^{\text{C}1}$ ), 124.73 ( $\text{C}^{\text{C}6/\text{C}8}$ ) and 121.25 ( $\text{C}^{\text{C}2}$ ) ppm.

#### 4.3. Thermogravimetry

Because the compounds **I** and **II** are planned to be used as precursors for the synthesis of coordination compounds through the solvothermal technique, it is very important to know its thermal stability, since this synthetic technique usually involves temperatures of about 150 °C or higher. To assess the stability of these compounds, thermogravimetric analyses were performed in the 30–550 °C range at a heating rate of 10 °C min<sup>-1</sup>. Fig. 4a and b shows the TG and DTG for compound **I** and **II** respectively. It can be observed that the ligand **I** is stable up to 280 °C, following, this compound decomposes vigorously until a temperature of 363 °C. For ligand **II**, the curve is divided into two stages. The first weight-loss process occurs around 100 °C, which can be attributed to the loss of lattice solvent molecules or it can also be imputed to a release of pyridine molecules (found 20%, calcd 18%). Subsequent to this, the ligand **II** remains thermally stable until is heated to 280 °C; then exhibits a rapid weight-loss process, corresponding to the

decomposition process of the organic ligand around 390 °C. Those results show that compounds **I** and **II** display excellent thermal stability.

#### 4.4. Photophysical properties

Knowledge about the orbital nature of our systems is important because many of the physical properties investigated depend on energy differences between frontier orbitals (i.e. HOMO, LUMO, SOMO). It is expected some differences in the luminescent behavior between pure compounds (**I** and **II** as ligands) and their respective coordination compounds, with transition metals. Therefore the photophysical properties of the compounds **I** and **II** have been investigated. Absorption spectra for ligands **I** and **II** in air-saturated dichloromethane solutions are shown in Fig. 5a. For ligand **I**, a well-defined band centered at 272 nm ( $\epsilon = 33.5 \times 10^3 \text{ M}^{-1} \text{ cm}^{-1}$ ) with a shoulder at 307 nm ( $\epsilon = 18.6 \times 10^3 \text{ M}^{-1} \text{ cm}^{-1}$ ) can be appreciated, while ligand **II** shows a structureless width absorption with a shoulder at 307 nm ( $\epsilon = 9.5 \times 10^3 \text{ M}^{-1} \text{ cm}^{-1}$ ). The absorbance maximum do not show any shift with solvent polarity, then these absorption bands could be attributed to a  $\pi \rightarrow \pi^*$  transition.

The terpyridyl species are well known for their versatile fluorescence properties at room temperature [12]. After excitation at 307 nm, emission bands can be appreciated for **I** and **II** at 372 and 407 nm, respectively (Fig. 5b). Table 2 summarizes the main photophysical properties. The quantum yield value for **I** was three times higher than for **II**. The vibrational structure of the each spectra and the short Stokes shift, can be explained due to the  $\pi \rightarrow \pi^*$  intramolecular fluorescence emission. The fluorescence lifetimes were 0.44 and 2.25 ns for compounds **I** and **II**, respectively.

#### 4.5. Density Functional calculations. DFT and TDDFT

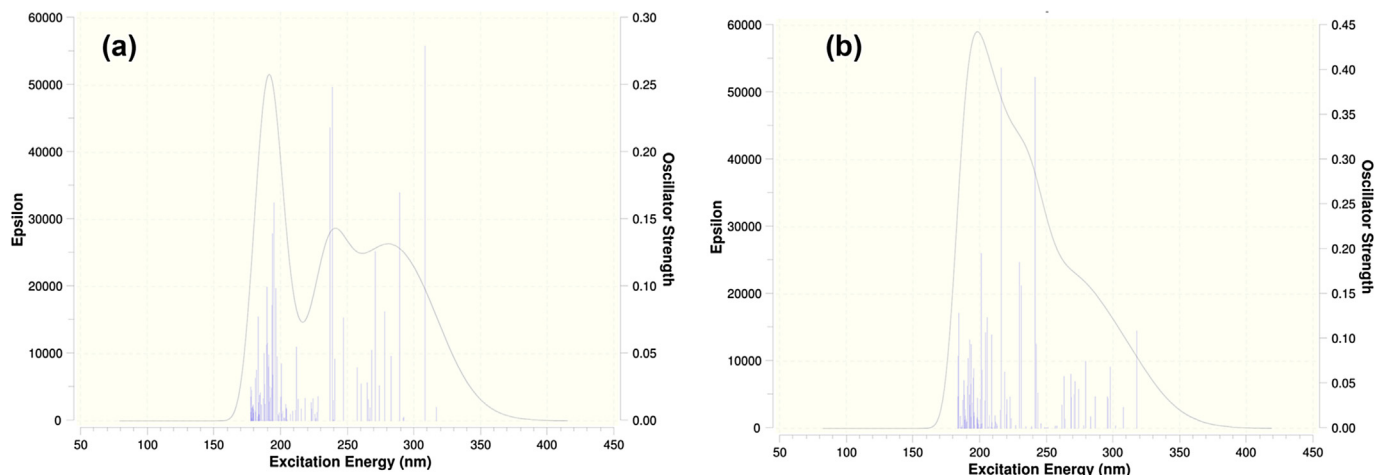
Density Functional calculations were performed in order to gain a better understanding of ligands photophysical properties. DFT calculations were used to optimize the geometry of compounds **I** and **II** in ground singlet state. Table S2 shows the very close agreement between the X-ray diffraction determined structure and the DFT-optimized geometry in gas phase. TDDFT allowed us to compute absorption spectra for **I** and **II** over the basis of the ground state optimized geometry. Fig. 6 shows the computed absorption spectra for **I** and **II**, making clear the close proximity to the experimental results.

Fig. 7 shows molecular orbital plots for **I** and **II**. Together with

**Table 2**

Summary of spectroscopic characterization of **I** and **II** in air-saturated  $\text{CH}_2\text{Cl}_2$  solutions.

Molecule	Absorption		Emission	
	$\lambda_{\text{max}} (\text{e}/10^3 \text{ M}^{-1} \text{ cm}^{-1})$	$\lambda_{\text{max}}$	$\Phi_{\text{em}} (10^{-2})$	$\tau (\text{ns})$
<b>I</b>	272 nm (33.5) 307 nm (18.6)	378 nm	3.2	0.44
<b>II</b>	307 nm (9.5)	407 nm	1.2	2.25



**Fig. 6.** Gas phase TDDFT computed absorption spectra for a.- I and b.- II.

**Table 3**, theoretical TDDFT results support the nature of the absorption as  $\pi \rightarrow \pi^*$ , and adds the information that correspond to intramolecular charge transfer.

The purpose behind this study is part of a larger research line, which seeks to compare the physical properties of molecules as free ligands and in their respective coordination compounds, particularly with paramagnetic ions.

## 5. Conclusion

Two new compounds, derivatives of terpyridine, were synthesized: 4'-(3-methyl-2-thienyl)-4,2':6',4''-terpyridine (**I**) and 4'-(4-

quinolinyl)-4,2':6',4''-terpyridine (**II**). Their molecular structures were obtained and their thermal stability was determined. Moreover, in order to compare with future compounds, their photochemical behavior was studied. The molecular orbitals involved indicate that the electronic transitions are  $\pi \rightarrow \pi^*$  type for both compounds. The theoretical studies show that these electronic transitions, involve different rings of the molecular structure for both compounds. Moreover, the differences in the chemical shifts observed in RMN experiences for the common terpyridine fragment probably are due to the different electron withdrawing capacity of the substituent groups. That is not clearly observed in the FTIR spectrum.

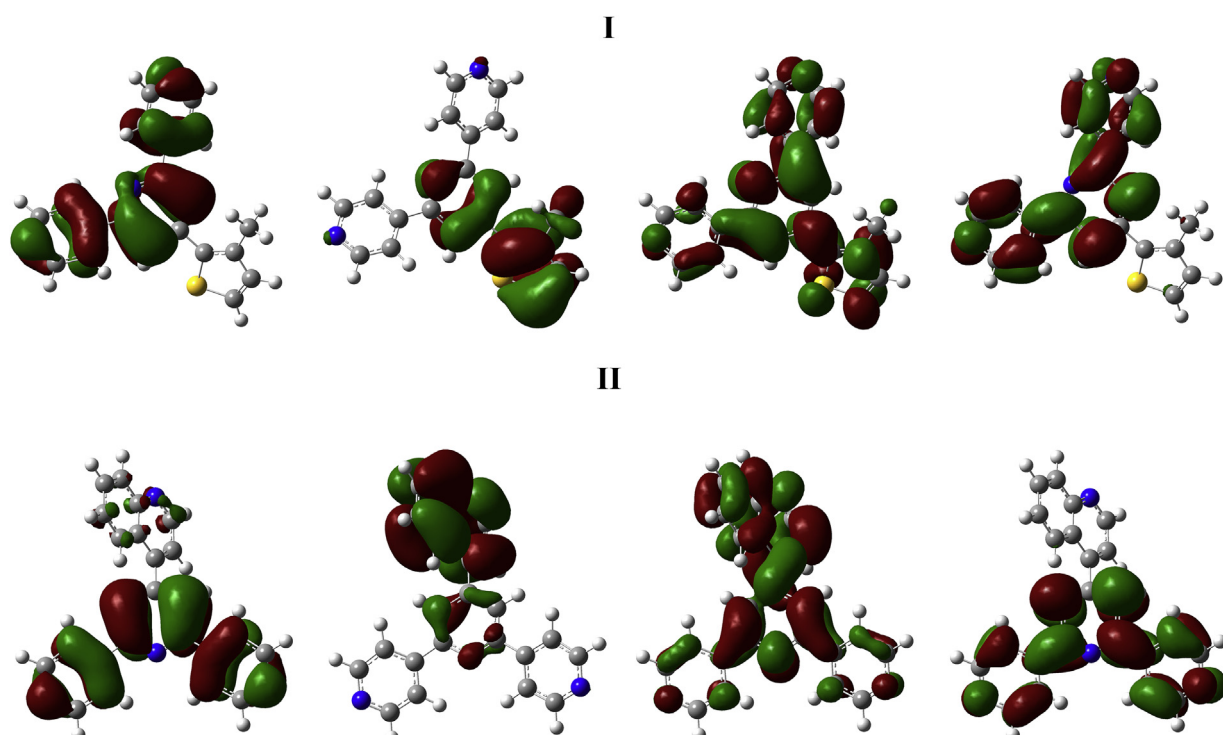


**Fig. 7.** DFT computed frontier orbitals HOMO-1, HOMO, LUMO and LUMO + 2 plots for **I** and **II**.

**Table 3**

Summary of main energy, wavelength and oscillator strength, computed for observed transitions in the absorption spectra of **I** and **II**, together with the orbitals implied.

N	E/eV	$\lambda/\text{nm}$	f	Major contributions
1				HOMO → LUMO (93%)
2	4.02	308	0.28	HOMO → LUMO + 1 (3%)
5	4.28	289	0.17	HOMO-7 → LUMO (10%)
				HOMO-7 → LUMO (3%)
				HOMO-1 → LUMO + 1 (62%)
				HOMO → LUMO + 1 (16%)
9	4.58	271	0.13	HOMO-7 → LUMO + 1 (4%)
				HOMO-2 → LUMO + 1 (12%)
				HOMO-2 → LUMO + 2 (14%)
				HOMO-1 → LUMO + 2 (37%)
17	5.02	247	0.08	HOMO → LUMO + 2 (93%)
21	5.19	239	0.25	HOMO-8 → LUMO + 2 (81%)
22	5.23	237	0.22	HOMO-1 → LUMO + 2 (89%)
55	6.35	195	0.16	HOMO-7 → LUMO + 3 (8%)
				HOMO-6 → LUMO + 3 (13%)
II				
1	4.03	318	0.11	HOMO → LUMO (95%)
9	4.43	280	0.08	HOMO-5 → LUMO (6%)
				HOMO-1 → LUMO + 1 (9%)
				HOMO → LUMO + 2 (71%)
16	4.62	269	0.06	HOMO-1 → LUMO + 1 (13%)
				HOMO-1 → LUMO + 2 (41%)
28	5.13	242	0.39	HOMO-6 → LUMO + 2 (45%)
				HOMO-9 → LUMO + 2 (26%)
33	5.36	231	0.16	HOMO-10 → LUMO (51%)
				HOMO → LUMO + 5 (22%)
34	5.39	230	0.19	HOMO → LUMO + 5 (49%)
				HOMO-10 → LUMO (15%)
41	5.73	216	0.40	HOMO-4 → LUMO + 2 (18%)
				HOMO → LUMO + 6 (25%)

Coordination polymers with 4'-(4-anthracen-9-yl)phenyl- and 4'-(naphthalene-1-yl)phenyl)-4,2':6',4"-terpyridines: mono-, di- and heptazinc(II) nodes, *Polyhedron* 62 (2013) 260–267.

- [5] E.C. Constable, G. Zhang, C.E. Housecroft, J.A. Zampese, Zinc(II) coordination polymers, metalloc hexacycles and metallocapsules—do we understand self-assembly in metallosupramolecular chemistry: algorithms or serendipity? *CrystEngComm* 13 (2011) 6864–6870.
- [6] J. Granijo, R. Gavino, E. Freire, R. Baggio, Monodentate and bridging behaviour of the sulfur-containing ligand 4'-[4-(methylsulfanyl)phenyl]-4,2':6',4"-terpyridine in two discrete zinc(II) complexes with acetylacetone, *Acta Crystallogr. Sect. C* 68 (2012) m269–m274.
- [7] L.-H. Cao, Q.-Q. Xu, S.-Q. Zang, H.-W. Hou, T.C.W. Mak, First three-dimensional self-penetrating coordination polymer containing rare (10,3)-d subnets: synthesis, structure, and properties, *Cryst. Growth Des.* 13 (2013) 1812–1814.
- [8] O.M. Yaghi, M. O'Keeffe, N.W. Ockwig, H.K. Chae, M. Eddaoudi, J. Kim, Reticular synthesis and the design of new materials, *Nature* 423 (2003) 705–714.
- [9] J.-P. Zhang, Y.-B. Zhang, J.-B. Lin, X.-M. Chen, Metal azolate frameworks: from Crystal engineering to functional materials, *Chem. Rev.* 112 (2011) 1001–1033.
- [10] X. Zhu, Q. Chen, Z. Yang, B.-L. Li, H.-Y. Li, Tuning zinc(II) coordination polymers based on bis(1,2,4-triazol-1-yl)ethane and 5-substituted 1,3-benzenedicarboxylates: syntheses, structures and properties, *CrystEngComm* 15 (2013) 471–481.
- [11] F. Allen, The Cambridge structural database: a quarter of a million crystal structures and rising, *Acta Crystallogr. Sect. B* 58 (2002) 380–388.
- [12] J. Costa, R. Ruloff, L. Burai, L. Helm, A.E. Merbach, Rigid  $\text{MIL}_2\text{Gd}_2\text{III}$  ( $\text{M} = \text{Fe}, \text{Ru}$ ) complexes of a terpyridine-based heteroditopic chelate: a class of candidates for MRI Contrast agents, *J. Am. Chem. Soc.* 127 (2005) 5147–5157.
- [13] B.-C. Wang, Q.-R. Wu, H.-M. Hu, X.-L. Chen, Z.-H. Yang, Y.-Q. Shangguan, M.-L. Yang, G.-L. Xue, Four novel  $\text{Zn}(\text{II})/\text{Cd}(\text{II})$  metal-organic frameworks constructed from 4[prime or minute]-4-pyridyl-4,2[prime or minute]:6[prime or minute]:4[double prime or minute]-terpyridine: hydrothermal synthesis, crystal structures, and luminescent properties, *CrystEngComm* 12 (2010) 485–492.
- [14] M. Barquín, J. Cancela, M.J. González Garmendia, J. Quintanilla, U. Amador, Coordination compounds of 4,2'-6',4"-terpyridine,  $[\text{MCl}_2(4,2'-6',4"-terpyridine)]$ ,  $\text{M} = \text{Mn}(\text{II}), \text{Co}(\text{II}), \text{Ni}(\text{II}), \text{Cu}(\text{II})$  or  $\text{Zn}(\text{II})$ . Crystal structure of catenapoly [(dichlorozinc)- $\mu$ -(4,2'-6',4"-terpyridine)], *Polyhedron* 17 (1998) 2373–2378.
- [15] E.C. Constable, G. Zhang, E. Coronado, C.E. Housecroft, M. Neuburger, Not just size and shape: spherically symmetrical d5 and d10 metal ions give different coordination nets with 4,2[prime or minute]:6[prime or minute]:4[double prime or minute]-terpyridines, *CrystEngComm* 12 (2010) 2139–2145.
- [16] M.-S. Wang, M.-X. Li, X. He, M. Shao, Z.-X. Wang, Synthesis, crystal structure and magnetic properties of two coordination polymers with 4-(4-carboxyphenyl)-4,2':6',4"-terpyridine ligand, *Inorg. Chem. Commun.* 42 (2014) 38–41.
- [17] J. Granijo, R. Gavino, E. Freire, R. Baggio, A novel hybrid terpyridine-pyrimidine ligand and the supramolecular structures of two of its complexes with  $\text{Zn}(\text{II})$  and acetylacetone: the underlying role of non-covalent  $\pi \cdots \pi$  contacts and C–H $\cdots$ X(O, N,  $\pi$ ) hydrogen bonds, *J. Mol. Struct.* 1063 (2014) 102–108.
- [18] G.A. Crosby, J.N. Demas, Measurement of photoluminescence quantum yields. Review, *J. Phys. Chem.* 75 (1971) 991–1024.
- [19] CrysAlis PRO, Oxford Diffraction Ltd., Yarnton, Oxfordshire, England, 2009.
- [20] G.M. Sheldrick, A short history of SHEXL, *Acta Crystallogr. Sect. A* 64 (2008) 112–122.
- [21] A. Spek, Structure validation in chemical crystallography, *Acta Crystallogr. Sect. D* 65 (2009) 148–155.
- [22] APEX2, Bruker AXS Inc., Wisconsin, USA Madison, 2001.
- [23] M.J. Frisch, G.W. Trucks, H.B. Schlegel, G.E. Scuseria, M.A. Robb, J.R. Cheeseman, G. Scalmani, V. Barone, B. Mennucci, G.A. Petersson, H. Nakatsuji, M. Caricato, X. Li, H.P. Hratchian, A.F. Izmaylov, J. Bloino, G. Zheng, J.L. Sonnenberg, M. Hada, M. Ehara, K. Toyota, R. Fukuda, J. Hasegawa, M. Ishida, T. Nakajima, Y. Honda, O. Kitao, H. Nakai, T. Vreven, J.A. Montgomery Jr., J.E. Peralta, F. Ogliaro, M. Bearpark, J.J. Heyd, E. Brothers, K.N. Kudin, V.N. Staroverov, R. Kobayashi, J. Normand, K. Raghavachari, A. Rendell, J.C. Burant, S.S. Iyengar, J. Tomasi, M. Cossi, N. Rega, N.J. Millam, M. Klene, J.E. Knox, J.B. Cross, V. Bakken, C. Adamo, J. Jaramillo, R. Gomperts, R.E. Stratmann, O. Yazyev, A.J. Austin, R. Cammi, C. Pomelli, J.W. Ochterski, R.L. Martin, K. Morokuma, V.G. Zakrzewski, G.A. Voth, P. Salvador, J.J. Dannenberg, S. Dapprich, A.D. Daniels, Ö. Farkas, J.B. Foresman, J.V. Ortiz, J. Cioslowski, D.J. Fox, Gaussian 09, Gaussian, Inc., Wallingford CT, 2009.

## Acknowledgment

The authors acknowledge to CONICYT Grant No. 21120148, FONDECYT 1130433 and LIA MIF-836 by partial financial support.

## Appendix A. Supporting information

Supporting information related to this article can be found at <http://dx.doi.org/10.1016/j.molstruc.2015.08.030>.

## References

- [1] E.C. Constable, R. Handel, C.E. Housecroft, M. Neuburger, E.R. Schofield, M. Zehnder, Efficient syntheses of 4'-(2-thienyl)- and 4'-(3-thienyl)-2,2':6',2"-terpyridine: preparation and characterization of Fe(II), Ru(II), Os(II) and Co(II) complexes, *Polyhedron* 23 (2004) 135–143.
- [2] E.C. Constable, C.E. Housecroft, P. Kopecky, M. Neuburger, J.A. Zampese, G. Zhang, Coordination polymers with divergent 4[prime or minute]:6[prime or minute]:4[prime or minute]:6[prime or minute]:4[prime or minute]:4[prime or minute]-terpyridine linkers: from aryl-aryl to ball-and-socket packing, *CrystEngComm* 14 (2012) 446–452.
- [3] E.C. Constable, C.E. Housecroft, M. Neuburger, J. Schönle, S. Vujošić, J.A. Zampese, Molecular recognition between 4'-(4-biphenyl)-4,2':6',4"-terpyridine domains in the assembly of d9 and d10 metal ion-containing one-dimensional coordination polymers, *Polyhedron* 60 (2013) 120–129.
- [4] E.C. Constable, C.E. Housecroft, J. Schönle, S. Vujošić, J.A. Zampese,